

Advantages of Backside Metal Contact Resistance on 4H-SiC Bonded Substrates for Power Devices

M. Kobayashi^{1,a*}, H. Uchida^{1,b}, N. Hatta^{1,c}, S. Ishikawa^{2,d},
Y. Higashi^{2,e}, H. Sezaki^{3,f}, S. Harada^{2,g}, and K. Kojima^{2,h}

¹SICOXS Corporation, 5-11-3, Shimbashi, Minato-ku,
Tokyo 105-0004, Japan

²Advanced Power Electronics Research Center, National Institute of Advanced Industrial Science and Technology (AIST), Tsukuba, Ibaraki 305-8568, Japan

³PHENITEC SEMICONDUCTOR Corp., 6833, Kinoko-cho, Ibara,
Okayama 715-8602, Japan

^{a*}motoki.kobayashi.x2@smm-g.com, ^bhidetsugu.uchida.x7@smm-g.com,
^cnaoki.hatta.x8@smm-g.com, ^dishikawa-seiji@aist.go.jp, ^ehigashi-phenitec@aist.go.jp,
^fhiroshi-sezaki@phenitec.co.jp, ^gs-harada@aist.go.jp, ^hkazu-kojima@aist.go.jp

Keywords: Bonded substrate, Backside metal contact resistance, Circular TLM, Temperature dependence

Abstract. A unique hybrid structure of the 4H-SiC bonded substrate offers advantages not achievable with conventional 4H-SiC bulk substrates, such as a reduction in on-state resistance and the suppression of forward bias degradation in power devices. This study focuses on the contact resistance between the polycrystalline layer and the backside metal (Ni/Ti) of 4H-SiC bonded substrates, along with its temperature dependence. The results indicate that the bonded substrates exhibit low backside contact resistance, even without annealing, and this resistance remains stable at elevated temperatures. Furthermore, power devices utilizing bonded substrates demonstrated reduced on-state resistance, as evaluated using Schottky barrier diodes (SBDs). Specifically, 4H-SiC bonded substrates without contact annealing lowered the forward voltage (VF) by 13% compared to 4H-SiC bulk substrates with contact annealing. These findings suggest that 4H-SiC bonded substrates simplify the backside contact process compared to 4H-SiC bulk substrates, offering significant benefits in reducing on-state resistance in SiC power devices.

Introduction

The 4H-SiC bonded substrate (SiCkrestTM), produced by SICOXS, consists of an ultra-thin (less than 1 μm) monocrystalline 4H-SiC layer bonded to an n-type low-resistivity polycrystalline 3C-SiC substrate using the surface-activated bonding method. This hybrid structure presents advantages not possible with traditional 4H-SiC bulk substrates, such as a reduction in on-state resistance[1] and the suppression of forward bias degradation in PiN diodes[2-3].

This study examines the contact resistance between the polycrystalline layer and the backside Ni/Ti metal of 4H-SiC bonded substrates. Given that the polycrystalline layer in bonded substrates exhibits extremely low resistivity (below 10 $\text{m}\Omega\cdot\text{cm}$), the objective is to investigate the differences in backside contact resistance and its temperature dependence between 4H-SiC bulk and 4H-SiC bonded substrates. Additionally, to assess the suitability of 4H-SiC bonded substrates with low-resistivity polycrystalline material and low backside contact resistance for power device applications, we fabricated SBDs on 4H-SiC bonded substrates.

Experimental

Fig. 1 presents the process flow and a schematic of the circular transmission line model (cTLM) structure used in this study. Three types of sample substrates were tested: (Sample a) 4H-SiC bulk substrates with contact annealing (annealed mono-SiC), (Sample b) 4H-SiC bonded substrates with contact annealing (annealed bonded-SiC), and (Sample c) 4H-SiC bonded substrates without contact annealing (unannealed bonded-SiC). The resistivity of the 4H-SiC bulk substrates and the polycrystalline layer of the 4H-SiC bonded substrates were approximately $20 \text{ m}\Omega\cdot\text{cm}$ and $10 \text{ m}\Omega\cdot\text{cm}$, respectively. Ti/Ni was used as the ohmic metal, and contact annealing was performed using rapid thermal annealing at 1200°C . The cTLM method was applied to measure backside contact resistance with high accuracy. In the cTLM technique, when the sum of radii ($r_1 + r_2$) is constant, the total resistance (R_T) between two electrodes depends linearly on the spacing parameter $= r_2 - r_1$. By fitting the measured R_T values for different d values, the sheet resistance (R_s) and the transfer length (L_T) can be determined. The specific contact resistance ρ_c is then calculated using $\rho_c = R_s L_T^2$ [4]. The cTLM pattern was designed with $r_1 + r_2$ constant and $r_2 - r_1 (=d)$ varying between 5 and $100 \mu\text{m}$. For I-V measurements, a Keithley B1505A was used, and the measurement temperature was controlled at room temperature (RT) and 175°C using a hot plate.

Fig. 2 outlines the process flow and schematic of the Schottky barrier diode (SBD) with a junction barrier Schottky structure, evaluated in this study. The same three types of sample substrates (SBD 1: annealed mono-SiC, SBD 2: annealed bonded-SiC, and SBD 3: unannealed bonded-SiC) were used for the SBD evaluation as for the cTLM assessments. The backside metal for the SBDs was Ti/Ni/Au, and the contact annealing conditions were the same as those used in the cTLM process. The forward current (IF)-forward voltage (VF) and reverse current (IR)-reverse voltage (VR) characteristics of the SBDs were measured.

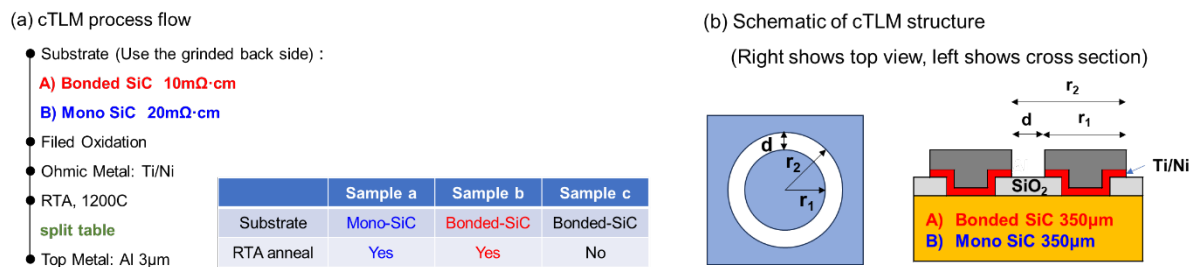


Fig. 1. (a) Process flow and (b) schematic image of the cTLM structure in this study.

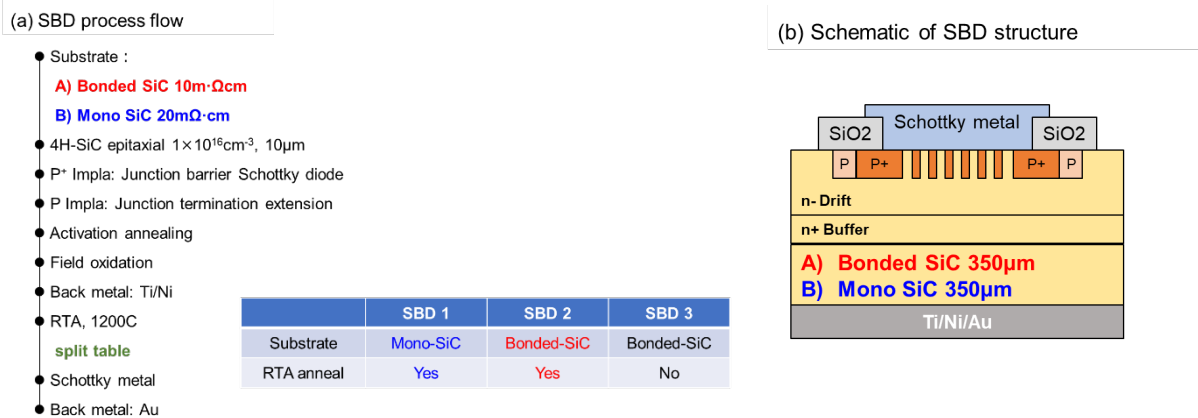


Fig. 2. (a) Process flow and (b) schematic image of the SBD structure in this study.

Results and Discussion

1. Backside contact resistance and its temperature dependence

Fig. 3(a) illustrates the I-V characteristics at $d = 100 \mu\text{m}$ for the cTLM measurements. All samples demonstrate ohmic contact behavior. Fig. 3(b) presents the TLM plots at RT. All samples exhibit good linearity in the TLM plots, and the contact resistance can be accurately measured using linear approximation. The slope and intercept for calculating the contact resistance were determined from the approximate equation at $d = 5\text{--}100 \mu\text{m}$.

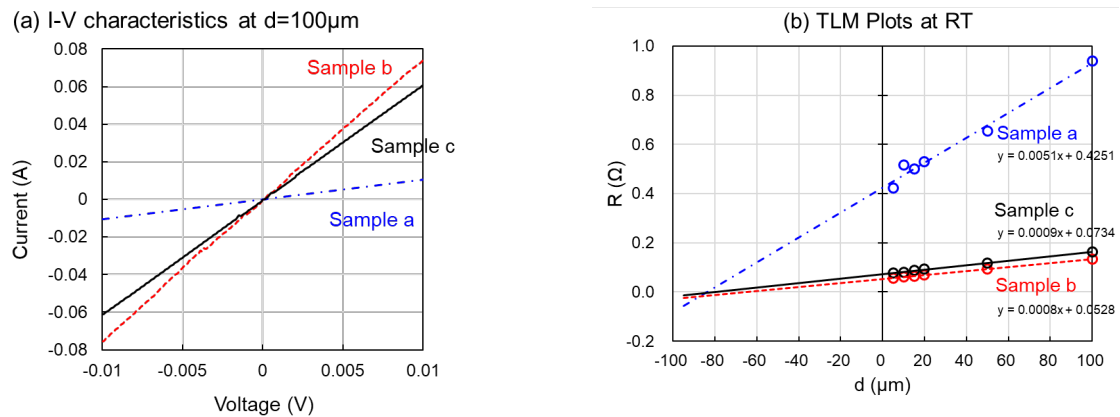


Fig. 3. (a) I-V characteristics at $d = 100 \mu\text{m}$ for the cTLM structure, and (b) TLM plots at room temperature (RT). Sample a represents annealed mono-SiC, sample b represents annealed bonded-SiC, and sample c represents unannealed bonded-SiC.

Fig. 4 displays the backside contact resistance at RT. The values of backside contact resistance for unannealed bonded-SiC are consistent with results from another research[5]. Unannealed bonded-SiC shows lower backside contact resistance compared to annealed mono-SiC, with annealed bonded-SiC demonstrating the lowest resistance. Notably, the contact resistance of unannealed bonded-SiC is an order of magnitude lower than the resistance of the polycrystalline material itself ($3.5 \times 10^{-4} \Omega \cdot \text{cm}^2$ at thickness of $350 \mu\text{m}$), indicating that the contact resistance is not a limiting factor. These findings confirm that low resistance backside contacts can be formed on 4H-SiC bonded substrates without annealing. Therefore, the elimination of the backside contact annealing process represents a key advantage of 4H-SiC bonded substrates.

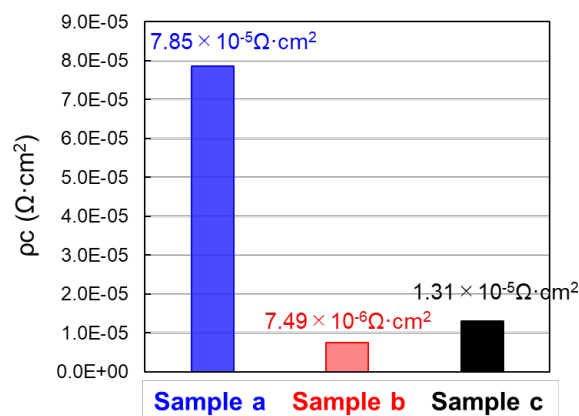


Fig. 4. Backside contact resistance at room temperature (RT). Sample a represents annealed mono-SiC, sample b represents annealed bonded-SiC, and sample c represents unannealed bonded-SiC.

Fig. 5 shows the backside contact resistance and the reduction ratio for each sample at both RT and 175°C. The contact resistance of annealed mono-SiC decreases at 175°C compared to RT, while the contact resistance of both bonded-SiC samples remains unchanged, demonstrating stability within this temperature range. Unannealed bonded-SiC reduces contact resistance by 83% at RT and 74% at 175°C compared to annealed mono-SiC. In addition to reducing backside contact resistance, the lack of temperature sensitivity provides another advantage of 4H-SiC bonded substrates.

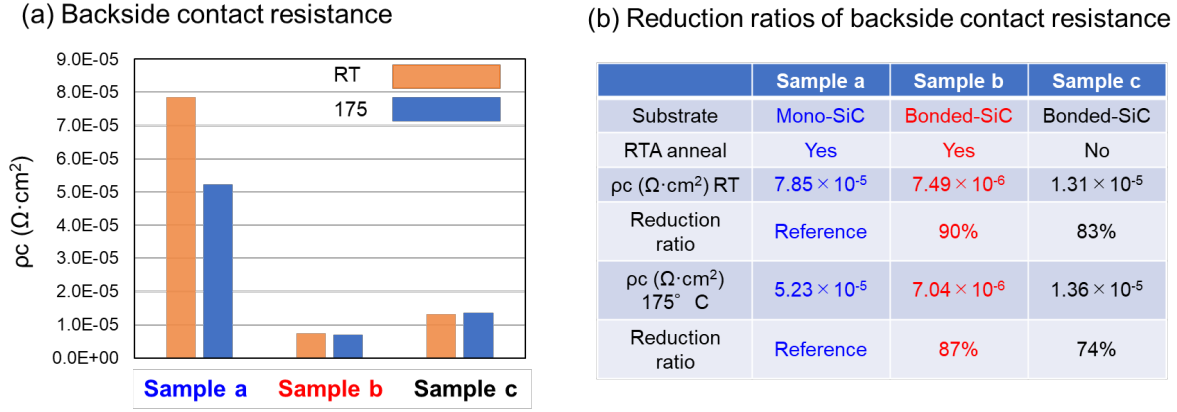


Fig. 5. (a) Backside contact resistance and (b) the reduction ratio of samples b and c at room temperature (RT) and 175°C, compared with sample a. Sample a represents annealed mono-SiC, sample b represents annealed bonded-SiC, and sample c represents unannealed bonded-SiC.

The difference in temperature dependence between the 4H-SiC bulk substrate and the 4H-SiC bonded substrates is discussed below. Equation 1 shows the relationship between substrate donor concentration and contact resistance[6].

$$\rho_c = \frac{1}{qA_{Ri}} \frac{k^2}{\sqrt{\pi(\phi_B + E_n) E_{00}}} \sqrt{\cosh\left(\frac{E_{00}}{kT}\right) \exp\left(\frac{\phi_B + E_n}{E_0} - \frac{E_n}{kT}\right)} \quad (1)$$

$$E_{00} = qh/4\pi \sqrt{\frac{N_D}{m_n^* \epsilon}} \quad (2)$$

In these equations, $E_0 = E_{00} \cosh(E_{00}/kT)$, and $A_{Ri} = 4\pi m_n^* q k^2_B / h^3$ is the Richardson constant. Here, h is the Planck constant, q denotes the electron charge, k is the Boltzmann constant, T is the absolute temperature, m_n^* is the effective electron mass, ϵ is the dielectric constant, ϕ_B is the barrier height for carrier transport, N_D is the electron carrier concentration (corresponding to the nitrogen concentration in the polycrystalline 4H-SiC bonded substrate), and E_n represents the energy difference between the conduction-band edge and the Fermi level of the semiconductor. The characteristic energy E_{00} is related to the tunneling probability for electrons in ohmic contacts.

It is expected that ρ_c is mainly determined by N_D and ϕ_B from Eq.1, and E_{00} is primarily determined by N_D from Eq.2. These relationships indicate that when tunneling current dominates ohmic contact behavior, the current in ohmic contacts depends on N_D . Conversely, if thermionic emission current dominates, the current depends on ϕ_B . Therefore, if tunneling current is the dominant mechanism in ohmic contacts, the temperature dependence diminishes.

Fig. 6 presents the fitting curves of temperature dependence for contact resistance, compared with the measured values of backside contact resistance (shown in Fig. 5). The fitting curve was calculated using Equation 1, with parameters adjusted to align with the measured values. From Fig. 6, the measured values closely follow the fitting curve, confirming that the strong temperature dependence of annealed mono-SiC is due to thermionic emission current in ohmic contacts. In contrast, the

minimal temperature dependence observed in bonded-SiC is predominantly influenced by tunneling current in the ohmic contact. Since the specific contact resistance ρ_c of bonded-SiC is primarily determined by the donor concentration (N_D) and is independent of the barrier height ϕ_B , the difference in ρ_c between bonded-SiC with and without contact annealing is negligible.

Based on the above discussion, the reduced temperature dependence of backside contact resistance in 4H-SiC bonded substrates can be attributed to the tunneling mechanism dominating the ohmic contact, driven by the high carrier concentration of the polycrystal. The polycrystalline layer of 4H-SiC bonded substrates has a higher nitrogen concentration (approximately $8.4 \times 10^{19} \text{ cm}^{-3}$) than the 4H-SiC bulk substrates (approximately $8 \times 10^{18} \text{ cm}^{-3}$).

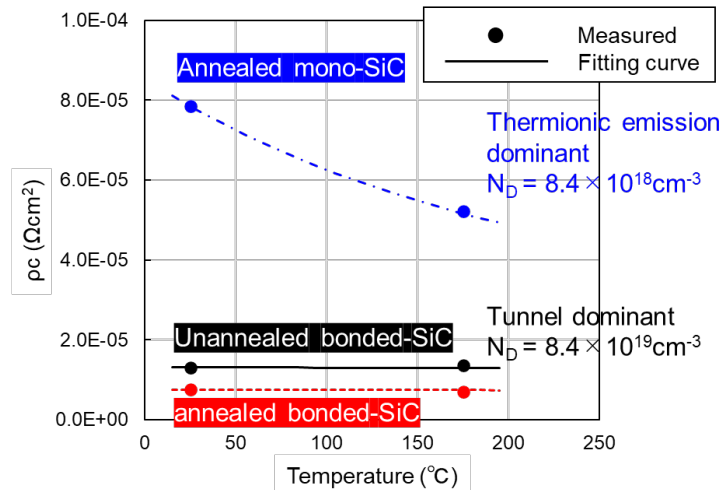


Fig. 6. Fitting curves of temperature dependence for contact resistance, compared with the measured values of backside contact resistance.

2. Effects of on-state resistance reduction evaluated by SBDs

Fig. 7 shows the (a) forward current (IF) - forward voltage (VF) characteristics and (b) VF at IF = 18 A for the SBDs, along with the corresponding reduction ratios. The VF of both annealed and unannealed bonded-SiC are equivalent and lower than that of annealed mono-SiC. Specifically, unannealed bonded-SiC reduces VF by 13% compared to annealed mono-SiC. Given that the backside contact resistance of bonded-SiC is very low ($1.31 \times 10^{-5} \Omega\text{cm}^2$ at RT for unannealed bonded-SiC), the difference in VF across the SBDs is primarily attributed to the low resistivity of the polycrystalline layer ($3.5 \times 10^{-4} \Omega\cdot\text{cm}^2$ at thickness of 350 μm). Fig. 8 presents the reverse current (IR)-reverse voltage (VR) characteristics of the SBDs. No significant difference is observed in the relationship between breakdown voltage and reverse leakage current. These results indicate that the 4H-SiC bonded substrate is highly advantageous for reducing the on-state resistance of SiC power devices.

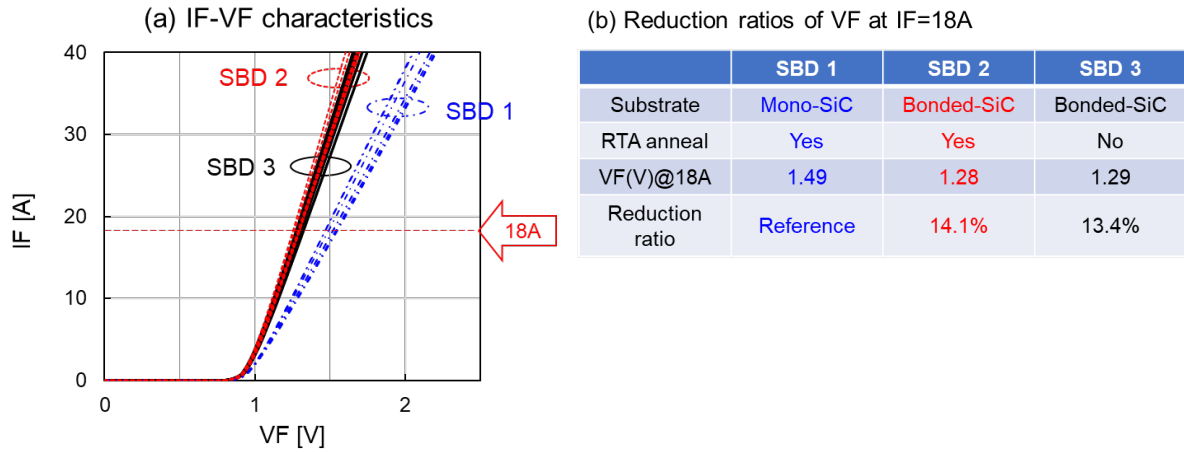


Fig. 7. (a) IF-VF characteristics and (b) VF at IF = 18 A for SBDs, along with the reduction ratio. SBD 1 represents annealed mono-SiC, SBD 2 represents annealed bonded-SiC, and SBD 3 represents unannealed bonded-SiC.

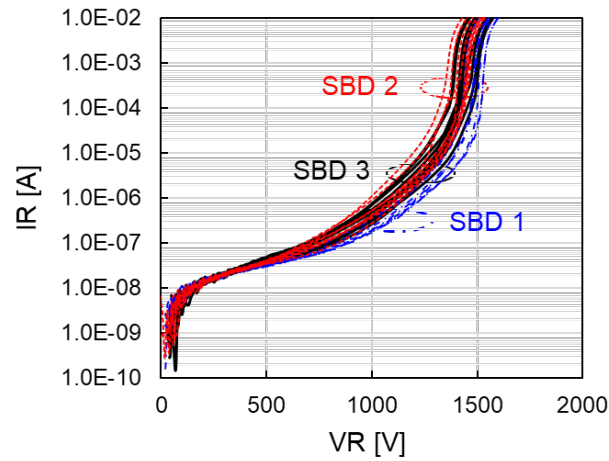


Fig. 8. IR-VR characteristics of SBDs. SBD 1 represents annealed mono-SiC, SBD 2 represents annealed bonded-SiC, and SBD 3 represents unannealed bonded-SiC.

Summary

In this study, we investigated the contact resistance between the polycrystalline layer and backside metal (Ti/Ni) of 4H-SiC bonded substrates, along with its temperature dependence. Backside metal contact resistance was measured with high accuracy using the cTLM method. The results revealed that the bonded substrates exhibit low backside contact resistance, even without annealing, and that the contact resistance remains stable at high temperatures. The reduced temperature dependence of backside contact resistance in 4H-SiC bonded substrates can be attributed to tunneling-dominant ohmic contact, driven by the high carrier concentration of the polycrystalline layer, which has a higher nitrogen concentration than that of 4H-SiC bulk substrates. In addition, the effects of on-state resistance reduction in power devices using 4H-SiC bonded substrates were evaluated through SBDs. Unannealed bonded-SiC reduced VF by 13% compared to annealed mono-SiC. These findings suggest that 4H-SiC bonded substrates can simplify the backside contact process compared to 4H-SiC bulk substrates and offer significant advantages in reducing the on-state resistance of SiC power devices.

Acknowledgements

This research was conducted under the joint research project of Tsukuba Power Electronics Constellations (TPEC). The co-authors, S. Ishikawa and Y. Higashi, are affiliated with PHENITEC SEMICONDUCTOR Corp.

References

- [1] T. Shimono, H. Uchida, A. Onogi, and H. Fujiwara, presented at the 7th Meeting on Advanced Power Semiconductors, Japan (2020)
- [2] N. Hatta, S. Ishikawa, K. Ozono, K. Masumoto, K. Yagi, M. Kobayashi, S. Kurihara, S. Harada, and K. Kojima, *Key Engineering Materials* 948, p. 107 (2023)
- [3] H. Uchida, M. Kobayashi, N. Hatta, S. Ishikawa, K. Ozono, K. Masumoto, S. Kurihara, S. Harada, and K. Kojima, *Abstract of 20th ICSCRM*, p. 209 (2023)
- [4] H. Kato, D. Takeuchi, N. Tokuda, H. Umezawa, H. Okushi, and S. Yamasaki, *Diamond and Related Materials*, 18, no. 5–8, pp. 782–785 (2009)
- [5] H. Biard, S. Odoul, W. Schwarzenbach, I. Radu, C. Maleville, A. Potier, M. Ferrato, and E. Guajioty, *Solid State Phenomena*, 1662-9779, 344, pp. 47-52 (2023)
- [6] Y. Liu, S. P. Singh, L. M. Kyaw, M. K. Bera, Y. J. Ngoo, H. R. Tan, S. Tripathy, G. Q. Lo, and E. F. Chora, *ECS Journal of Solid State Science and Technology*, 4, no. 2, pp. 30-35 (2015)